

This article was downloaded by:[TU Technische University Berlin]
On: 24 August 2007
Access Details: [subscription number 769788577]
Publisher: Taylor & Francis
Informa Ltd Registered in England and Wales Registered Number: 1072954
Registered office: Mortimer House, 37-41 Mortimer Street, London W1T 3JH, UK



International Journal of Electronics

Publication details, including instructions for authors and subscription information:
<http://www.informaworld.com/smpp/title~content=t713599654>

Gain modulation of unbiased semiconductor lasers: ultrashort light-pulse generation in the 0.8 μm -1.3 μm wavelength range

D. Bimberg ^a; K. Ketterer ^a; E. H. Böttcher ^a; E. Scöll ^b

^a Institut für Festkörperphysik 1 der Technischen Universität Berlin, Berlin 12,
Germany

^b Institut für Theoretische Physik der RWTH-Aachen, Aachen, Germany

Online Publication Date: 01 January 1986

To cite this Article: Bimberg, D., Ketterer, K., Böttcher, E. H. and Scöll, E. (1986)
'Gain modulation of unbiased semiconductor lasers: ultrashort light-pulse generation
in the 0.8 μm -1.3 μm wavelength range', International Journal of Electronics, 60:1,
23 - 45

To link to this article: DOI: 10.1080/00207218608920760
URL: <http://dx.doi.org/10.1080/00207218608920760>

PLEASE SCROLL DOWN FOR ARTICLE

Full terms and conditions of use: <http://www.informaworld.com/terms-and-conditions-of-access.pdf>

This article maybe used for research, teaching and private study purposes. Any substantial or systematic reproduction, re-distribution, re-selling, loan or sub-licensing, systematic supply or distribution in any form to anyone is expressly forbidden.

The publisher does not give any warranty express or implied or make any representation that the contents will be complete or accurate or up to date. The accuracy of any instructions, formulae and drug doses should be independently verified with primary sources. The publisher shall not be liable for any loss, actions, claims, proceedings, demand or costs or damages whatsoever or howsoever caused arising directly or indirectly in connection with or arising out of the use of this material.

© Taylor and Francis 2007

Gain modulation of unbiased semiconductor lasers: ultrashort light-pulse generation in the 0.8 μm –1.3 μm wavelength range

D. BIMBERG†, K. KETTERER†, E. H. BÖTTCHER†
and E. SCHÖLL‡

Stable production of 15 ps pulses having a peak power of 200 mW from fully gain-modulated, unbiased GaAs double-heterostructure and multiple-quantum-well lasers emitting in the 0.8 μm –0.9 μm wavelength range and from InGaAsP double heterostructure lasers emitting in the 1.2 μm –1.3 μm range is reported. The shortest pulses obtained from GaAs DH lasers show a width as small as 2 ps. The optical pulses represent the first relaxation oscillation of the laser. Special double avalanche generators are developed to produce large injection-current pulses with widths down to 125 ps at repetition rates up to 10 MHz. Numerical and approximate analytical solutions of a coupled-rate-equation model of a semiconductor laser incorporating bimolecular recombination and realistic injection current pulse shapes are presented. The theoretical predictions are found to be in excellent agreement with the experimental results.

1. Introduction

The development of sources for the generation of 2–15 ps light pulses in the 0.8–1.3 μm wavelength range from *unbiased gain-modulated* semiconductor lasers is reported in this paper.

High-speed semiconductor light sources generating ultrashort pulses with a half-width of a few picoseconds and a peak power equal to or possibly larger than the CW power are essential for a broad range of quite different applications. These applications include high-bit-rate optical communication, ultrafast optical signal processing, optical sources for optical electronics, ps time-resolved spectroscopy, optical printer, optical disc, digital audio disc and laser ranging.

Following the development in other areas of quantum electronics, it has been well established for a number of years that picosecond and subpicosecond pulses can be obtained by active or passive mode locking of semiconductor laser diodes in external cavities (Ho *et al.* 1978, Ito *et al.* 1980, Holbrook *et al.* 1980, Ippen *et al.* 1980, van der Ziel *et al.* 1981, van der Ziel 1981, Tsang *et al.* 1983, Lundquist *et al.* 1983). With active mode locking a pulse width of 5.3 ps has been obtained (van der Ziel 1981), while with passive mode locking pulses as short as 0.65 ps were reported (van der Ziel *et al.* 1981). For most important applications, however, such pulses are quite impractical, since they are always emitted in a continuous train without the possibility of a large variation of the repetition frequency. Gating of individual pulses has been achieved only recently (Tsang *et al.* 1983) by using the quite

Received 25 April 1985; accepted 12 June 1985.

† Institut für Festkörperphysik I der Technischen Universität Berlin, Hardenbergstraße 36, 1000 Berlin 12, Germany.

‡ Institut für Theoretische Physik der RWTH-Aachen, Templergraben 52, 5100 Aachen, Germany.

complex arrangement of a cleaved-coupled-cavity (C^3) laser. Furthermore, an external cavity has to be used, which is difficult to adjust and sensitive to temperature variations and/or mechanical vibrations. The length of the external cavity determines the repetition rate.

Gain switching by direct modulation of the injection current is the other basic method for producing ultrashort optical pulses. No external cavity is needed, and the repetition rate can be easily varied up to an f_{\max} which depends on some of the properties like the threshold current I_t of the particular laser used for the experiments and on the characteristics of the injection-current circuit. Using normal GaAs and InGaAsP double-heterostructure lasers, pulse widths of 25 ps–35 ps have been obtained (Ito *et al.* 1979, White *et al.* 1985, Lin *et al.* 1984, Onodera *et al.* 1984) by prebiasing the laser to values $0.5I_t$ – $2I_t$, and superimposing a high-frequency current.

It is worth pointing out that Fourier-transform-limited single-mode ($\Delta\lambda = 0.7$ nm) pulses of 35 ps width were observed from InGaAsP distributed feedback lasers. (Onodera *et al.* 1984). Coherence is apparently not degraded by short pulse generation if a suitable laser of advanced technology is utilized. No systematic search, however, for pulses of minimum width was reported in this work.

A prebias of the order of $0.5I_t$ – $2I_t$, has at least two basic disadvantages. The laser is continuously subjected to heating from the bias current. The amplitude of the additional current pulses that can be employed is thus limited to avoid thermal destruction and the lifetime of the laser is degraded. Furthermore, there is a continuous emission of incoherent or coherent light, depending on this bias, which is most unwelcome for almost any applications.

Direct AC excitation is actually simpler and avoids these drawbacks. Pulse widths of 28 ps (Au Yeung 1981) and—most excitingly—repetition frequencies up to 11 GHz have been reported recently (Lau *et al.* 1984, 1985) for most advanced GaAs window buried heterostructure lasers on a semi-insulating substrate. No pulse-width measurements were reported for the latter case. The half-width of the injecting sine half-wave depends of course on the repetition frequency. Thus the pulse width of the optical pulse changes with the repetition frequency. This disadvantage can be avoided by employing discrete pulse generators producing short electrical pulses with an on/off ratio much less than one.

Preliminary experiments with unbiased proton-implanted double-heterostructure GaAs lasers which were triggered by single avalanche generators at a repetition rate of up to 10 MHz lead to the observation of 23 ps pulses (Klein *et al.* 1982 b). These were the shortest pulses produced hitherto by gain modulation of a semiconductor laser. A theoretical analysis (Schöll *et al.* 1984) identified that the first relaxation oscillation (and, depending on the injection current, subsequent ones) of the laser accounts for the short optical pulses observed. A number of theoretical simulations of the light output of a conventional GaAs DH laser under various injection conditions suggested that generation of 10 ps pulses having a peak power of 100 mW or more should be feasible if the laser is triggered electrically in such a way that only the first relaxation oscillation is emitted. Indeed, reproducible generation of such pulses has now been achieved for three completely different types of lasers in both the 0.8 – 0.9 μm and 1.2 – 1.3 μm wavelength ranges, as will be reported in this paper.

The paper is organized as follows. In §2 the theoretical background is briefly summarized. The results of further numerical simulations based on realistic parameters of GaAs double-heterostructure (DH) and multiple-quantum-well (MQW)

lasers are given, together with analytical solutions for the dependence of the delay time between electrical and optical pulse, the pulse width and the peak power on the amplitude of the injection current pulse. Although these solutions are approximate, and thus quantitatively less accurate than numerical solutions, they provide deeper physical insight.

The generation of the electrical pump pulses and the detection of the optical output pulses of the lasers in two completely different wavelength ranges are the key experimental issues of this work, and will be reported in §§3 and 4. Pulse detection in the 0.8–0.9 μm range is performed using a single-shot streak camera with high temporal resolution and subsequent digital data acquisition. A fast Ge/GaAs heterostructure photodetector in conjunction with a fast sampling scope is used for detection in the 1.2–1.3 μm range.

In §5 we report results on ps-pulse generation employing GaAs DH, GaAs MQW and InGaAsP DH lasers. For the first time we observe from all lasers stable 10–15 pulses, and in the case of the GaAs DH laser even 2 ps pulses, using gain switching *without* prebias. Some preliminary results of GaAs DH lasers were recently given elsewhere (Bimberg *et al.* 1984).

2. Theory

First the fundamentals of a non-linear-rate-equation model developed recently by Schöll *et al.* (1984) are summarized. This model is numerically evaluated, inserting injection-current pulse shapes that approximate the experimental ones and varying a number of fundamental laser and excitation parameters. One result of general importance is the existence of a maximum current density amplitude J_{opt} for a given injection current shape and a given laser: J_{opt} is defined as that current density for which the optical peak power is maximum, the halfwidth of the first relaxation oscillation is minimum, and simultaneously the second and higher relaxation oscillations are suppressed. Then we present approximate analytical solutions for the four most important quantities: the photon peak power N_{max} , the delay time T between the first and second relaxation oscillation, the delay time τ_d between the electrical and the optical pulse, and the width t_{FWHM} of the first relaxation oscillation.

The emission of a semiconductor laser is modelled by a set of coupled rate equations for the temporal evolution of the photon density N and the electron density n (Schöll *et al.* 1984). Mode couplings and the diffusion of carriers are neglected. The following processes are taken into account:

- (i) Stimulated emission and absorption of rate gN , where $g = \tilde{B}(n - n_{\text{th}})$ is the gain, n is the electron density in the n-doped laser active region, and n_{th} is the carrier density to achieve transparency; N is the photon density;
- (ii) spontaneous emission into the lasing mode of rate Bnp , where $p = n - N_D$ is the hole concentration in the laser active region; we have assumed an effective donor density N_D ;
- (iii) non-radiative transitions and spontaneous emission into non-lasing modes of rate Dnp ;
- (iv) photon dissipation by cavity loss, scattering, etc., of rate κN ;
- (v) pumping through a time-dependent injection-current pulse of given current density $J(t)$.

Other excitation processes like thermal excitation are neglected. \tilde{B} , B and D are rate constants of dimension $\text{cm}^3 \text{s}^{-1}$, κ^{-1} is the photon lifetime (in s).

The resulting rate equations are

$$\dot{N} = \tilde{B}(n - n_{\text{th}})N + B(n - N_{\text{D}})n - \kappa N \quad (1a)$$

$$\dot{n} = \frac{J(t)}{eL} - \tilde{B}(n - n_{\text{th}})N - (B + D)(n - N_{\text{D}})n \quad (1b)$$

where e is the elementary charge and L is the thickness of the laser active layer. The electron density n_t and the injection current density J_t at the CW laser threshold are

$$n_t = n_{\text{th}} + \kappa/\tilde{B} \quad (2)$$

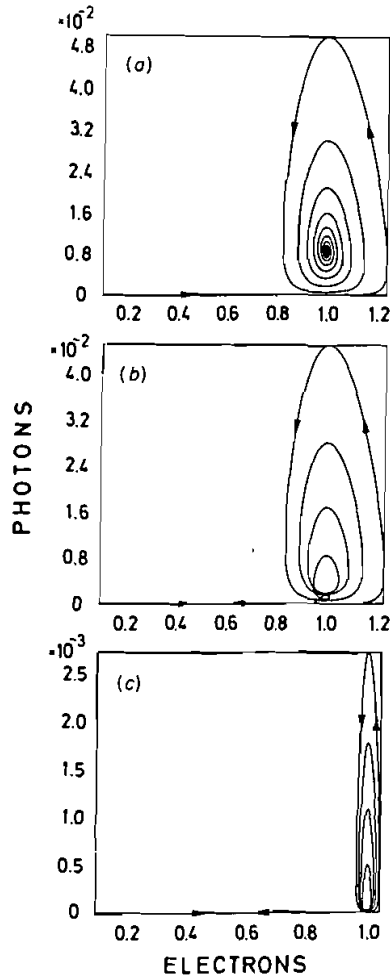


Figure 1. Phase portraits of photons and electrons with (a) step-function injection current $J_0 = 8.6J_t$, (b), (c) J gaussian with $J_0 = 8.6J_t$, $t_0 = 500$ ps, $t_r = 250$ ps, $t_f = 280$ ps. The material parameters are $D = 1.5 \times 10^{-10} \text{cm}^3 \text{s}^{-1}$, $B/D = 10^{-3}$, $n_{\text{th}} = 1.3 \times 10^{18} \text{cm}^{-3}$ and (a), (b) $n_t = 6.5 \times 10^{18} \text{cm}^{-3}$, $N_{\text{D}} = 6.5 \times 10^{17} \text{cm}^{-3}$, $\kappa^{-1} = 1.25$ ps, (c) $n_t = 2.6 \times 10^{18} \text{cm}^{-3}$, $N_{\text{D}} = 2.0 \times 10^{17} \text{cm}^{-3}$, $\kappa^{-1} = 0.2$ ps. The trajectory corresponding to the initial thermal equilibrium $N = 0$, $n = N_{\text{D}}$ is shown. The electron and photon densities are in units n_t .

and

$$J_i = (B + D)n_i(n_i - N_D)eL \quad (3)$$

We have computed numerical solutions of (1) for a number of material parameters and different shapes of the applied injection current pulse. Figure 1 shows phase portraits of the electron and photon densities $n(t)$, $N(t)$ for two different injection currents and two different sets of material parameters, corresponding to typical values for GaAs double-heterostructure lasers (Boers *et al.* 1975, Chik *et al.* 1980, Hwang *et al.* 1973). Figures 1(a) and (b) are plotted with $D = 1.5 \times 10^{-10} \text{ cm}^3 \text{ s}^{-1}$, $B/D = 10^{-3}$, $\tilde{B} = 1.5 \times 10^{-7} \text{ cm}^3 \text{ s}^{-1}$, $N_D = 6.5 \times 10^{17} \text{ cm}^{-3}$, $\kappa^{-1} = 1.25 \text{ ps}$, $n_{\text{th}} = 1.3 \times 10^{18} \text{ cm}^{-3}$, which yields $n_i = 6.5 \times 10^{18} \text{ cm}^{-3}$ and $J_i = 2.7 \times 10^4 \text{ A cm}^{-2}$ ($L = 0.3 \mu\text{m}$).

Figure 1(c) is plotted with the same values of D , B/D , n_{th} , but with smaller values of the donor concentration and the photon lifetime ($N_D = 2 \times 10^{17} \text{ cm}^{-3}$, $\kappa^{-1} = 0.2 \text{ ps}$, $\tilde{B} = 3.8 \times 10^{-6} \text{ cm}^3 \text{ s}^{-1}$), which yields $n_i = 2.6 \times 10^{18} \text{ cm}^{-3}$ and $J_i = 0.45 \times 10^4 \text{ A cm}^{-2}$ ($L = 0.3 \mu\text{m}$). These values are representative for the lasers used here.

The phase portraits of Figs. 1(a)–(c) show the flow $n(t)$, $N(t)$ of electrons and photons starting at time $t = 0$ from the phase point ($n = N_D$, $N = 0$). This point corresponds approximately to thermal equilibrium, where the electron density is equal to the doping concentration, and the photon density is negligible. Figure 1(a) represents the case of a step-function injection-current density. The time delay between the instantaneous increase of electron density and the delayed response of the photon density is clearly seen. The relaxation oscillations and the decrease of their amplitude with increasing time towards a steady-state value are nicely visualized. It should be noted that the current density chosen for this phase portrait is 8.6 times the threshold current density J_i . The highest value the electron density reaches ($\approx 1.2n_i$) is much below that ratio.

Figures 1(b) and (c), in contrast, represent the transient case of an injection current pulse. An asymmetric gaussian is chosen, in order to allow for rise and decay times t_r and t_f respectively, independent of each other. The current density is

$$J(t) = \begin{cases} J_0 \exp \{ -[(t - t_0)/t_r]^2 \} & \text{for } t < t_0 \\ J_0 \exp \{ -[(t - t_0)/t_f]^2 \} & \text{for } t \geq t_0 \end{cases} \quad (4)$$

approximating well the experimentally used current shape (see § 3). The peak current density versus threshold ratio $J_0/J_i = 8.6$ is the same as in Fig. 1(a); $t_r = 250 \text{ ps}$ and $t_f = 280 \text{ ps}$ are used. The phase portrait shows that, in contrast with Fig. 1(a), fewer relaxation oscillations occur, decaying faster in amplitude. Finally the system in the phase plane relaxes from $n = n_i$, $N \approx 0$ to the initial equilibrium point $n = N_D$, $N = 0$ along the n -axis. This corresponds to the decay of the electrons to thermal equilibrium on the slow time-scale $(DN_D)^{-1}$.

A comparison of the first relaxation oscillation of Fig. 1(a) with the first relaxation oscillation of Fig. 1(b) discloses a great similarity. Indeed, numerical calculations with a large number of different injection-current pulse shapes show that the shape of the first relaxation pulse is largely independent of the rise time of the current, as long as the time when the peak injection current occurs is roughly matched to the delay time.

Figure 2 shows the normalized photon density of the laser pulses (relaxation oscillations) versus time for various peak current densities J_0 and fall times t_f , and

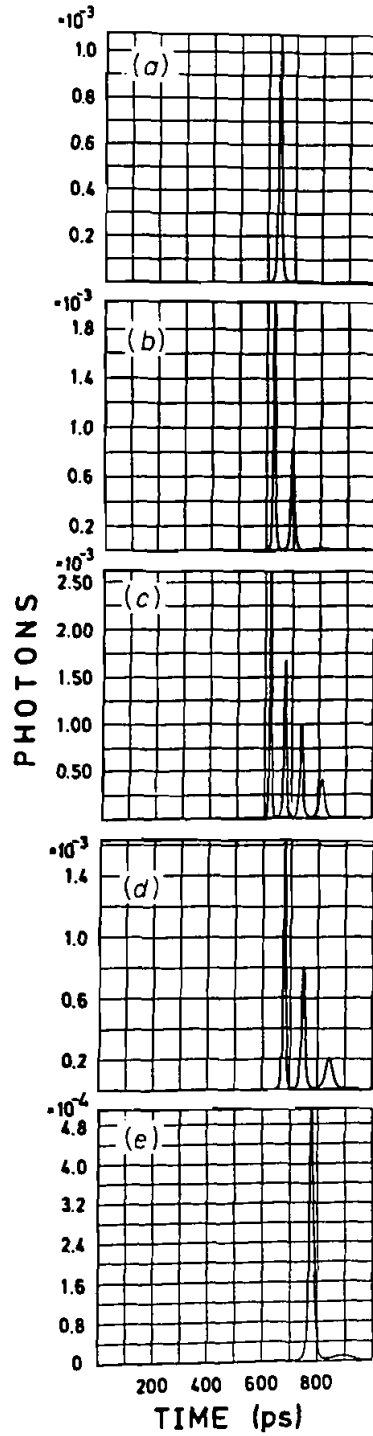


Figure 2. Photon concentration in units of n , versus time as numerical solution of the rate equations (1) with the same material parameters as in Fig. 1(c). The injection current is modelled as gaussian according to (4) with $t_0 = 500$ ps, $t_r = 250$ ps. (a) $t_r = 150$ ps, $J_0 = 8.6J_1$; (b) 200 ps, $8.6J_1$; (c) 280 ps, $8.6J_1$; (d) 280 ps, $7.6J_1$; (e) 280 ps, $6.7J_1$.

the same material parameters as Fig. 1(c). In Figs. 2(a)–(c) t_f increases from 150 ps to 280 ps at constant J_0 , and in Figs. 2(c)–(e) J_0/J_1 decreases at constant t_f from 8.6 to 6.7. For values of $t_f < 150$ ps at $J_0/J_1 = 8.6$, or values of $J_0/J_1 < 6.5$ at $t_f = 280$ ps, no laser oscillations occur at all. For a sufficiently slow current falltime t_f and sufficiently large J_0/J_1 , several relaxation oscillations are emitted (Figs. 2(b)–(d)). The peaks of these successive oscillations increase with increasing J_0/J_1 , and increasing t_f . The relative magnitude of successive peaks decreases here more rapidly than after step-function excitation, and their halfwidth becomes successively broader.

In Fig. 3 photon and electron densities are shown together with the injection-current pulse for a wider range of peak current densities J_0 and the same current shape as in Figs. 2(c)–(e). The large increase in the number and the peak values of the laser spikes with increasing J_0 is nicely seen. In Fig. 4 an analogous plot is presented for a different injection-current pulse shape with a faster decay appropriate to experiments reported here (cf. Fig. 9 below). There exists a minimum value j_0^{\min} of j_0 , considerably larger than the CW threshold $j_0 = 1$, below which no laser emission occurs. This effective threshold of the laser at which light emission occurs is pulse-shape dependent and is much higher in Fig. 4 than for the longer pulses of Fig. 3. On the other hand, the first relaxation oscillation is narrower, and the contrast (peak ratio of the 1st and 2nd oscillation) is much larger.

For a Gaussian pulse shape (4) the width (FWHM) of the current pulse $t_{1/2}$ is related to t_r and t_f by

$$t_{1/2} = (\ln 2)^{1/2}(t_r + t_f) = 0.83(t_r + t_f) \quad (5)$$

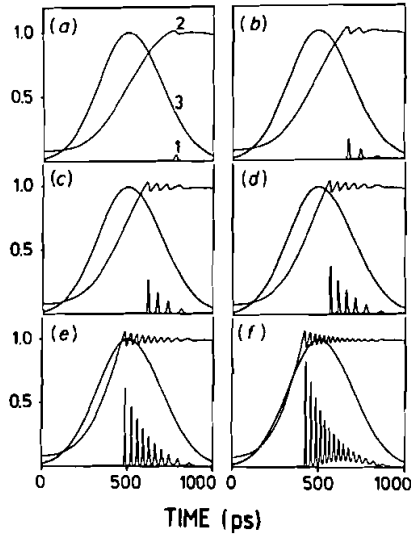


Figure 3.

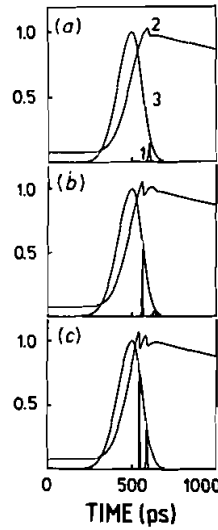


Figure 4.

Figure 3. Photon concentration N (curve 1), electron concentration n (curve 2), and injection current J (curve 3) versus time for the material parameters of Fig. 1(c) (numerical solution). The injection current is modelled as gaussian according to (4) with $t_0 = 500$ ps, $t_r = 250$ ps, $t_f = 280$ ps. N is in units of $n_1/100$, n is in units of n_1 , and J in units of J_1 . (a) $J_0 = 6.7J_1$; (b) $7.6J_1$; (c) $8.6J_1$; (d) $10J_1$; (e) $14J_1$; (f) $20J_1$.

Figure 4. Same as in Fig. 3, but with $t_r = 120$ ps, $t_f = 83$ ps. (a) $J_0 = 16J_1$; (b) $18J_1$; (c) $20J_1$.

With the material parameters of Fig. 2, the 'effective laser threshold' j^{\min} corresponds to $j^{\min} \approx 15$ for $t_{1/2} = 170$ ps (Fig. 4), $j^{\min} \approx 8.5$ for $t_{1/2} = 330$ ps (Fig. 2(a)) and $j^{\min} \approx 6.5$ for $t_{1/2} = 440$ ps (Fig. 2(e)). For much longer $t_{1/2}$ j^{\min} tends to the CW value $j_0 = 1$, while for much shorter $t_{1/2}$ the minimum peak injection current j^{\min} becomes infinite, i.e. no laser action is possible for any peak current, because the duration of the current pulse is too short to drive the electron density beyond the threshold value n_t . The shift of the effective laser threshold j^{\min} with $t_{1/2}$ as predicted by our model is in good agreement with our experimental findings (Fig. 15). With increasing ratio $j_0 = J_0/J_t$ in the range $6 \leq j_0 \leq 25$:

- (i) the FWHM of the first relaxation oscillation decreases sharply well below 10 ps;
- (ii) the delay time τ_d of the first light pulse decreases slowly but remains at several hundred picoseconds;
- (iii) the time difference T between subsequent relaxation oscillations decreases down to the 40 ps range, depending on the details of the exciting current pulse;
- (iv) the peak power (proportional to the peak photon density N_{\max}) of the laser pulses increases less than linearly.

Figures 5(a)–(d) show explicitly the dependence of delay time τ_d , the spacing of the first two relaxation oscillations T , the width of the photon pulse t_{FWHM} and the amplitude of the first relaxation oscillation N_{\max} on the normalized peak injection-current density for the material parameters and current pulse shape of Fig. 1(c). Of

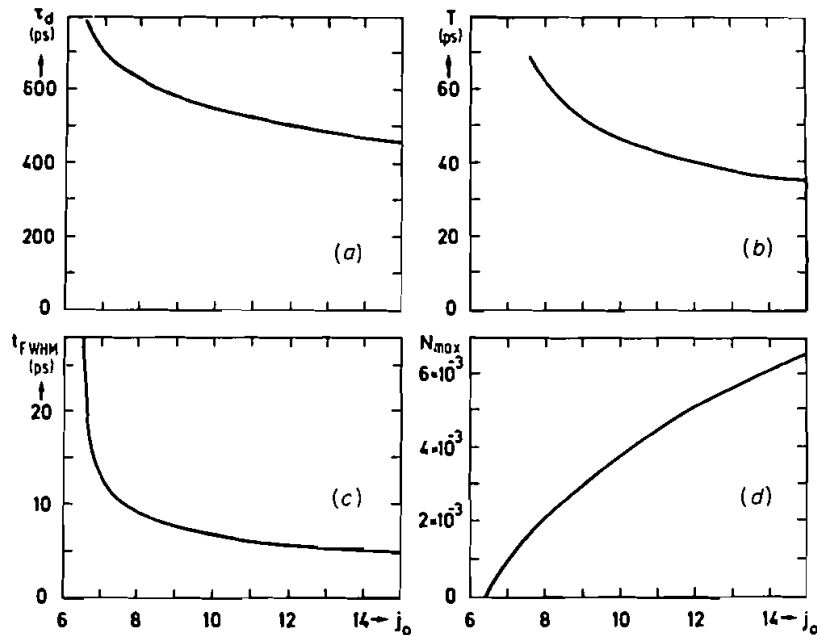


Figure 5. Delay time τ_d , width of the photon pulse t_{FWHM} , spacing of the first two relaxation oscillations T , and amplitude of the first relaxation oscillation N_{\max} (= peak power in arbitrary units) as a function of j_0 (numerically calculated, $j_0 = J_0/J_t$; parameters as in Fig. 1(c)).

course the absolute values of the quantities shown here depend largely on material parameters of the laser.

We would like to emphasize at this point one important consequence of these results for all practical applications. For a given laser and a given injection pulse shape there exists *exactly one* peak current density J_{opt} that produces a single light pulse with optimized properties—minimum halfwidth and maximum peak intensity. Just one relaxation oscillation is emitted for J_{opt} . For $J > J_{\text{opt}}$ the second and higher relaxation oscillations appear, and for practical applications the ‘effective halfwidth’ of the asymmetrical envelope of the pulse train has to be used, which is of course much larger than the halfwidth of the first relaxation oscillation at $J = J_{\text{opt}}$. For $J < J_{\text{opt}}$ the pulse amplitude rapidly decreases and the halfwidth increases according to Fig. 5. Comparing Figs. 3 and 4, it is evident that J_{opt} depends strongly on the injection pulse shape. The injection pulses of Fig. 4 result in much narrower pulses than the pulses of Fig. 3.

We have also used other sets of material parameters in order to check the sensitivity of our numerical results to these values. In Fig. 6 the relative spontaneous emission coefficient B/D has been varied. An increase of the spontaneous emission coefficient B/D by a factor of 10 (Fig. 6(a)) increases t_{FWHM} by one third and decreases N_{max} by one third for $j_0 = 10$. Further increase of B/D eventually suppresses the relaxation oscillations altogether—an effect that has already been pointed out previously (Boers *et al.* 1975).

Variation of the doping concentration N_D over several orders of magnitude (Fig. 7) produces only slight changes in the laser pulses. For instance, by increasing N_D from 4×10^{16} to 10^{18} cm^{-3} , the pulse width t_{FWHM} is increased from 6.5 to 8.5 ps at

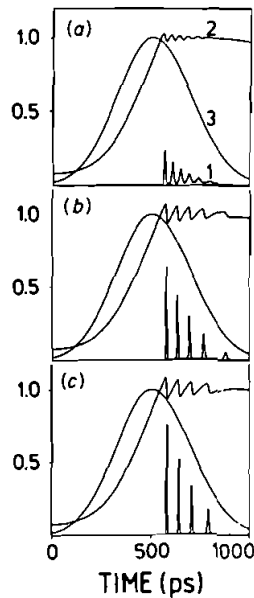


Figure 6.

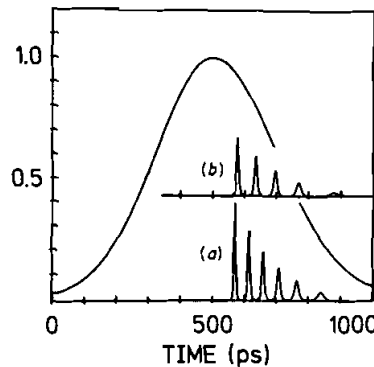


Figure 7.

Figure 6. Same as in Fig. 3, with $J_0 = 10J_1$ and B/D varied: (a) $B/D = 10^{-2}$; (b) 10^{-4} ; (c) 10^{-6} .

Figure 7. Same as in Fig. 3, with $J_0 = 10J_1$ and N_D varied: (a) $N_D = 4 \times 10^{16} \text{ cm}^{-3}$; (b) 10^{18} cm^{-3} .

$J_0 = 10J_t$. An increase of D or κ decreases all relevant times significantly (τ_d , T , t_{FWHM}).

In order to gain deeper physical insight into the mechanism of the laser pulse generation, we have obtained analytical expressions for the delay time and the width of the laser pulse (Schöll *et al.* 1984). First, solutions of (1) in terms of phase portraits for the flow $n(t)$ and $N(t)$ (Fig. 1) are discussed in more detail.

Neglecting spontaneous emission into the lasing mode ($B = 0$), the steady-state (n^* , N^*) of (1) for a constant current is given by

$$N^* = 0, \quad n^* = \frac{N_D}{2} \left[1 + \left(1 + \frac{4J}{(B+D)N_D^2 eL} \right)^{1/2} \right] \quad (6a)$$

for $J < J_t$ (below threshold) and by

$$N^* = \frac{J - J_t}{\kappa eL}, \quad n^* = n_t \quad (6b)$$

for $J > J_t$. For fixed J the flow of photons $N(t)$ and of electrons $n(t)$ is always directed towards the appropriate steady state, which is therefore always stable.

The question of the path in the (n, N) -plane by which the steady state (n^* , N^*) is approached can be answered by linearizing around this steady state and solving the rate equations explicitly in its neighbourhood. For physically reasonable material parameters, all trajectories spiral around the steady state (N^* , n^*) in the phase plane.

For a time-dependent J the whole flow picture of the phase portrait changes as time passes on. Hence, in contrast with the standard phase portraits for autonomous systems of differential equations, a trajectory $(n(t), N(t))$ can intersect itself as shown in Fig. 1(b).

Initially, at $t = 0$ we have $J = 0$, and hence by (6) the steady state is $N^* = 0$, $n^* = N_D$. As J increases, the steady state first moves along the n -axis, and then, above threshold, along the line $n = n_t$, by (6). The flow is directed away from the initial point $N^* = 0$, $n^* = N_D$ as indicated in Fig. 1. The increase of photons by (1a) is negligible as long as $n < n_t$ and the electron number $n(t)$ increases by (1b) with $N \equiv 0$. If the current density $J(t)$ rises sufficiently fast on the time-scale of the electronic transitions, the phase point $(n(t), N(t))$ remains at sufficient distance from the actual steady state (n^* , N^*) in the phase plane. Hence the recombination term in (1b) may be neglected, and $n(t)$ is given approximately by

$$n(t) = N_D + Dn_t(n_t - N_D) \frac{J_0}{J_t} \int_0^t f(t') dt' \quad (7)$$

where $f(t)$ is the current shape function.

The delay time τ_d for the onset of the photon pulse can be defined by $n(\tau_d) = n_t$. For a step-function injection current, i.e. instantaneous rise of the current to its maximum value, it follows from (7) that

$$\tau_d^{\text{step}} \approx (Dn_t J_0/J_t)^{-1} \quad (8)$$

For current pulses with a finite rise time, such as in (4), one finds

$$\tau_d \approx \tau_d^{\text{step}} = \tau_d^0$$

where τ_d^0 is the asymptotic value of τ_d for large $j_0 = J_0/J_t$, and depends upon the detailed pulse shape, but not on the peak value j_0 .

Quite generally, the approximations (8), (9) are valid for large j_0 as used in our experiments. Owing to the neglect of recombination, the approximate delay times are slightly too small. For the parameters appropriate to our experiments (see caption of Fig. 1(c)) the error as compared with the numerical solution (Fig. 3(a)) is 8% for $j_0 = 7$, 5% for $j_0 = 7.6$ and below 2% for $j_0 \geq 10$. Note that in the case of step currents more sophisticated expressions for τ_d are available (t Hooft 1981, Dixon *et al.* 1979).

For $n > n_t$ stimulated emission becomes effective, and the photon number increases. Relaxation oscillations are initiated. During each of these the current $J(t)$ may be approximated by an appropriate constant value J . From (1), linearized around the steady state (n^*, N^*) for fixed $J \approx J_0$, one finds oscillatory solutions $\delta N(t)$, $\delta n(t) \sim \exp(-\lambda t) \exp(-i\omega t)$ ($\delta N := N - N^*$; $\delta n := n - n^*$) with damping constant

$$\lambda = \frac{D}{\kappa} \left[(2n_t - N_D) \left(1 - \frac{n_{th}}{n_t} \right) + (n_t - N_D)(j_0 - 1) \right] \quad (10)$$

and period

$$T = \frac{2\pi}{\omega} = 2\pi \left[\frac{n_t - n_{th}}{(n_t - N_D) D n_t \kappa (j_0 - 1)} \right]^{1/2} \quad \text{for } DN_D \ll \kappa n_t / (n_t - n_{th}) \quad (11)$$

Thus in a linear approximation the first relaxation oscillation for $\lambda \ll \omega$ would be approximately an ellipse centred around the steady state (n^*, N^*) in the phase portrait with peak photon density $2N^*$. However, from the phase portrait (Fig. 1(a)) it is obvious that the peak photon concentration N_{max} is drastically increased by the non-linearities in (1), such that the FWHM becomes essentially shorter than $T/2 = \pi/\omega$. This effect is the stronger, the larger j_0 is.

An approximation of the non-linear FWHM can be computed by retaining, in the photon rate equation, in addition to the terms arising from the linearization around (n^*, N^*) , the full non-linear gain and loss terms. An exact first integral of the rate equations can then be obtained. If the second integration is carried out approximately up to lowest order in the small parameter $N^*/\delta N$, the following FWHM is found:

$$t_{FWHM} \approx 0.8 \left[\frac{N^*}{N_{max} - N^*} \right] \frac{T}{2} \quad (12)$$

For Fig. 2(c), for instance, this means $f_{FWHM} \approx 0.4 \times T/2$.

Obviously this approximation is good if $N^*/(N_{max} - N^*)$ is small, i.e. for a large overshoot of N_{max} over N^* , as is the case for large j_0 . For the parameters appropriate to our experiments there is excellent agreement with the numerical result, the error being less than 6% for $j_0 \geq 7.6$ in Fig. 3(c).

Alternative approximations of t_{FWHM} were given by van der Ziel and Logan (1982) for combined DC and microwave current injection. Their analytical approximations are valid for DC currents close to threshold ($j_0 = 1$), and are thus complementary to our calculations.

The peak photon concentration N_{max} and thus the relative peak optical power can be calculated approximately from the non-linear rate equations:

$$N_{max} = N^* + \frac{N^*}{j_0 - 1} \ln \frac{N^*}{N(\tau_d)} \quad (13)$$

where $N(\tau_d)$ corresponds to the photon density at CW threshold. $N(\tau_d)$ is governed by the spontaneous emission factor B/D , and increases with increasing ratio B/D .

3. Electrical pulse generation

The numerical simulations of §2 have shown that the halfwidth, the intensity ratio and the number of the relaxation oscillations depend on the detailed shape—in particular the fall time t_f of the current pulse. A number of different single and double avalanche generators were developed by us to allow for experiments with widely varying current pulse rise and fall times.

Single avalanche generators similar to the one described by Klein *et al.* (1982*b*) can be used to produce pulses of width larger than 400 ps and amplitudes of 15–20 V. Much larger amplitudes up to 50 V and halfwidths down to 125 ps are produced with double avalanche generators of the outlay displayed in Fig. 8. 50 Ω microstrip lines on epoxy material are used. The length of the pulses is essentially determined by the length of the load line of the second transistor and by the length of the strip of the short circuit. For a given length of the load line the falling edge of the pulse can be modelled and made steeper by a suitable superposition of the primary and the reflected wave, i.e. by a proper choice of the short-circuit microstrip length. The transistors used are selected commercial types allowing for a maximum repetition rate f_{\max} of 5 ... 10 MHz.

This limit is imposed by the rapidly increasing amount of heat dissipated in the circuit, and is certainly still orders of magnitude below the maximum repetition rate of the laser. Preliminary experiments with other types of circuits showed that f_{\max} is certainly higher than 0.5–1 GHz. The avalanche circuit is triggered directly by a Wavetek 191 pulse generator. The amplitude of the injection pulse is varied by inserting commercial microwave attenuators in steps of 0.5 dB between the laser and the pulse generator.

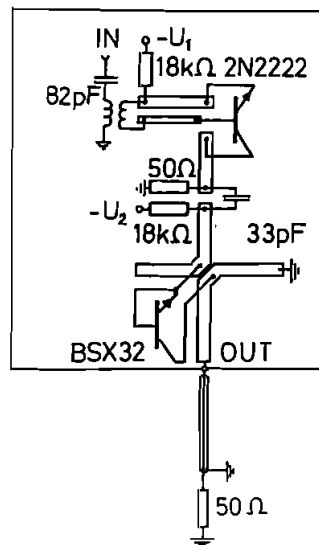


Figure 8. Layout of the double avalanche generators used for the injection pulse generation.

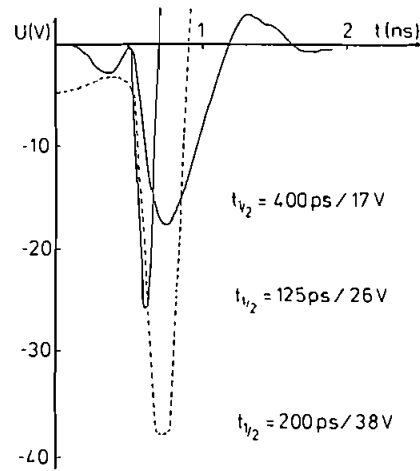


Figure 9. Voltage/time dependence of three typical injection pulses used in the course of these experiments produced by a simple avalanche generator ($t_{1/2} = 400$ ps) and by double avalanche generators ($t_{1/2} = 200, 125$ ps).

In Fig. 9 typical pulses of two different double avalanche generators are shown together with a pulse from a single avalanche generator. The pulses from the double avalanche generators show two peculiarities which turned out to be helpful:

- a small precursor pulse, and
- a fast switching from negative to positive voltage (forward to reverse bias).

The pulse shapes were measured on a $50\ \Omega$ load using a fast-sampling oscilloscope. The actual current pulses that inject charge carriers into the active region of the laser have a shape different from the voltage pulses. The electrical characteristics of the laser, in particular the depletion and the diffusion capacitance and the actual I - V dependence have to be taken into account. Typical values of the depletion and the diffusion capacitances are 40 – 100 pF and 5 nF respectively. A time delay between the voltage and the current occurs, mainly due to the depletion capacitance. Both types of capacitance modify the rise and decay times, in opposite ways.

Figure 10 shows the result of a numerical simulation. The voltage pulse having a halfwidth of 200 ps is taken from Fig. 9 (without precursor). Figure 10(a) shows the

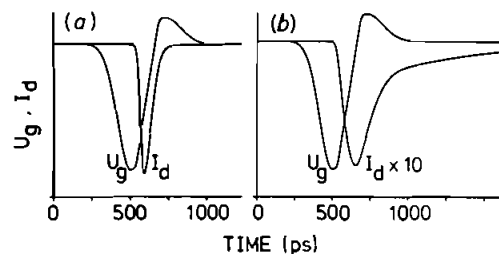


Figure 10. Pulse generator voltage U_g and calculated laser diode current I_d assuming (a) depletion capacitance of unbiased pn-junction $C_s = 100$ pF; (b) $C_s = 100$ pF and diffusion capacitance $C_d = 5$ nF. Inclusion of C_s results in a phase shift of I_d relative to U_g . Inclusion of C_d additionally strongly damps and broadens I_d .

pulse-narrowing effect of the depletion capacitance, and Figure 10(b) shows the broadening effect of the diffusion capacitance. The small positive (reverse) pulse after the main pulse helps to shorten the current decay time. The precursor (its effect is not shown here for sake of simplicity) reduces the delay between current and voltage pulse.

4. Optical pulse detection

Injection lasers emitting in the wavelength regions $0.8\text{--}0.9\ \mu\text{m}$ and $1.2\text{--}1.3\ \mu\text{m}$ are investigated. Two completely different types of experiment are used to detect the optical pulses in the different regions.

4.1. A single-shot streak-camera system

Figure 11 shows a block diagram of the optical pulse generation and detection system employing a single-shot streak-camera system. The pulse generator was discussed in §3. The laser, connected to the avalanche generator by a microstripline technique, is placed on a Peltier element permitting the control of the temperature between 0°C and 70°C with a resolution of 0.1°C . This Peltier element does not only help to avoid thermal heating effects. It also allows a continuous control of the peak injection current to threshold current ratio. This ratio is coarsely controlled and altered in steps by inserting commercial microwave attenuators between the laser and the pulse generator. Fine control is achieved by a variation of the laser temperature via the Peltier element. The threshold current of a laser shows an exponential temperature dependence. This fine tuning turned out to be crucial for a number of experiments, as will be seen in §5.

The light output of the laser is focused onto the screen of a Hadland Imacon 500 single-shot streak camera with S25 extended-red cathode having a sensitivity of $5.6\ \text{mA/W}$ at $800\ \text{nm}$. The camera is fibreoptically coupled to a 'streak intensifier' consisting of a channelplate. The signal of the streak intensifier is finally detected by

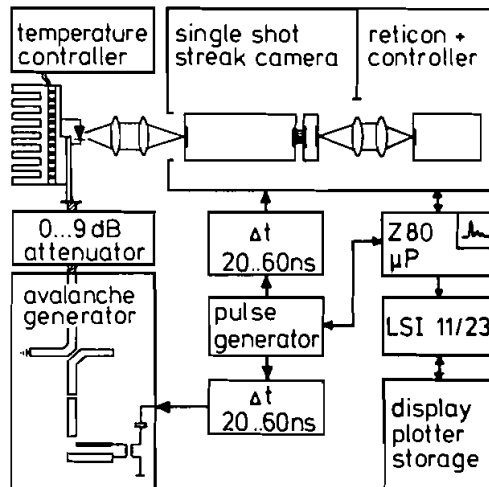


Figure 11. Block diagram of computer-controlled single-shot streak-camera set-up with $1.8\ \text{ps}$ time resolution.

a 512 pixel reticon from Princeton Instruments, which is again equipped with a channelplate. The total system sensitivity allows the detection of about 10^3 photons in a single 2 ps pulse at this wavelength. The time resolution of the present system is 1.8 ps.

The signal from the reticon is rapidly transferred to a Z80 microprocessor acting as a buffer, and eventually stored, plotted, displayed, averaged etc. using a DEC LSI 11/23 computer with multiuser operating system. A trigger logic selects single pulses from a variable-frequency pulse generator to trigger the streak camera via a variable delay in such a way that the optical pulse falls into the streak window.

4.2. A fast semiconductor photodetector system

The sensitivity of the photocathode of the present streak camera drops sharply towards zero at ≈ 900 nm. For longer laser wavelengths a different detection system is employed, based on a semiconductor photodetector (see Fig. 12). This photodetector (see inset on Fig. 13) consists of a $2.6 \mu\text{m}$ thick layer of nominally undoped Ge ($n \approx 2 \times 10^{17} \text{ cm}^{-3}$), grown on top of a semi-insulating GaAs substrate by vapour-phase epitaxy (Kräutle *et al.* 1983). The dimensions of the photosensitive area are restricted to $6 \mu\text{m} \times 30 \mu\text{m}$ by contact and mesa etching. The structure and the mounting of this germanium photodetector are similar to those of the planar GaAs and $\text{Ga}_x\text{In}_{1-x}\text{As}$ photodetectors, reported previously by Klein *et al.* (1982*a*). A voltage of 6 V is applied to the photodetector by means of a broadband microwave bias network (HP 33150 A).

Microscope objectives are used to focus the laser light on the sensitive area of the photodetector. The size of the laser spot on the detector surface is viewed by an IR sensitive vidicon and is adjusted to a diameter of about $3 \mu\text{m}$. In order to determine the response of the detection system independently of the laser pulses under investigation, it was tested using narrow test pulses of known width emitted by a GaAs multiple-quantum-well (MQW) laser (see § 5.2). The rise time and halfwidths of these laser pulses are measured by the single-shot streak camera. Figure 13 shows the response for such MQW-laser pulses. The response of the system is neither gaussian nor lorentzian of shape, but rather is asymmetric. A detailed analysis of the complete detection circuit was made (and is described elsewhere: Bimberg *et al.* 1985) and leads to a somewhat complex analytical formula for the time dependence of its response to a photon pulse of finite width. Without such an analysis a meaningful deconvolution of the detector response to varying laser signals would not be

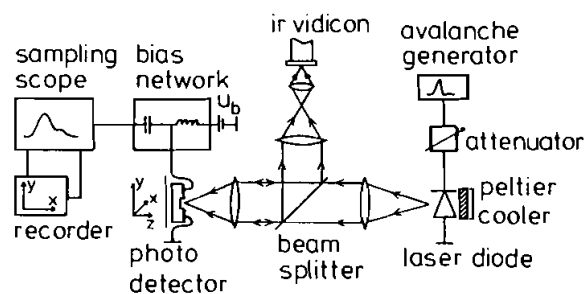


Figure 12. Block diagram of a photodetector-based set-up for the detection of infrared picosecond pulses.

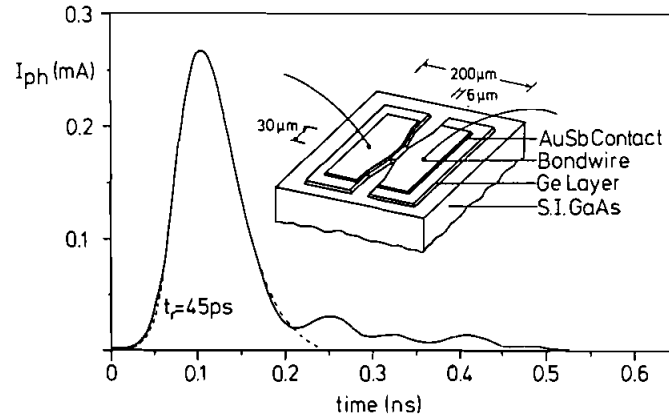


Figure 13. Photocurrent response I_{ph} of the photodetection system (germanium photodetector, see Fig. 12) to a multiple-quantum-well laser pulse of 26 ps risetime and 33 ps FWHM. The insert shows schematically the detector design. The full line represents the experimental result; the dashed line represents our numerical fit, which is based on an analysis of the complete detection circuit.

possible. The comparison of the measured response to the MQW-laser pulse (full line in Fig. 13) with the calculated one (dashed line in Fig. 13) demonstrates the precision of our theoretical description.

5. Properties of the laser pulses

Three different types of lasers have been employed so far for short pulse generation:

GaAs/GaAlAs V-groove and MQW lasers emitting in the 0.8–0.9 μm wavelength range, and

InGaAsP V-groove lasers emitting in the 1.2–1.3 μm wavelength range.

Some of the most important results for these three laser types will be presented now.

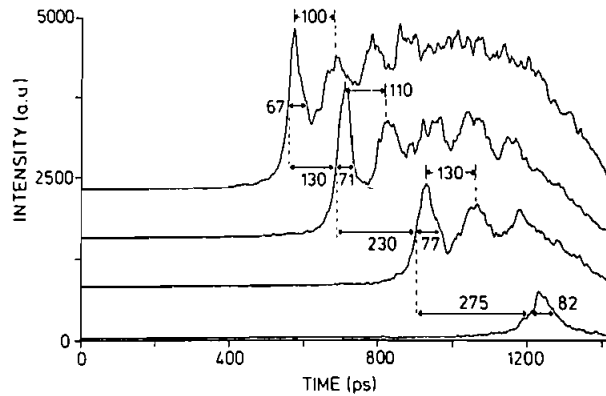


Figure 14. Emission of a GaAs/DH V-groove laser after excitation with current pulses of $t_{1/2} = 2$ ns. The attenuation of the pulses decreases from bottom to top from 15 dB to 12 dB in steps of 1 dB, corresponding to $J_0 = 4.5J_t, 4J_t, 3.4J_t, 3J_t$.

5.1. GaAs/GaAlAs V-groove lasers

The lasers used here are of a commercial DH V-groove type manufactured by AEG-Telefunken. The Al content of the active layers is $\approx 3\%$, resulting in an emission wavelength of $\approx 840\text{ nm}$; the cavity length is $\approx 340\ \mu\text{m}$. The emission at DC excitation of $I = 1.2I_t$ contains approximately 10 modes; typical threshold currents for CW operation are $I_t \approx 80\text{ mA}$.

Figure 14 shows 4 different optical pulses emitted from such a laser held at a temperature of 22°C after excitation with $2\text{ ns}/40\text{ V}$ pulses attenuated by $12 \dots 15\text{ dB}$, respectively. The time resolution of the streak camera is set to 15 ps . Just one relaxation oscillation, $t_{\text{FWHM}} = 82\text{ ps}$ wide, is emitted at 15 dB attenuation. After an increase of the current by 1 dB two more relaxation oscillations show up. The first relaxation oscillation has gained a factor of 3 in intensity and has a reduced width of 77 ps . The delay time τ_d between electrical and optical pulse is reduced by 275 ps . This trend continues with increasing injection current:

t_{FWHM} decreases,
 τ_d decreases,
 the delay T between first and second relaxation oscillation becomes shorter,
 the peak power of the first relaxation oscillation increases in perfect agreement with the theoretical predictions (see Fig. 5).

Figure 15 shows the minimum peak injection current J^{min} for laser activity for this laser at 10°C as a function of the width of the electrical pulses. For very narrow electrical pulses the threshold increases sharply and goes to infinity—again in agreement with theory.

A variation of the injection current for a given pulse shape by fixed attenuators only is too coarse and not sufficient to find the optimum condition for minimum laser pulse width. We have therefore in addition varied the temperature of the laser. Thus the CW threshold of the laser is varied together with the ratio of peak current to threshold current. The threshold increases with increasing temperature. Figure 16 shows 4 optical pulses after excitation with $200\text{ ps}/40\text{ V}$ injection pulses attenuated by 6 dB . The laser is held at temperatures of $30^\circ, 25^\circ, 20^\circ, 10^\circ\text{C}$ respectively. The time resolution of the streak camera is 1.8 ps .

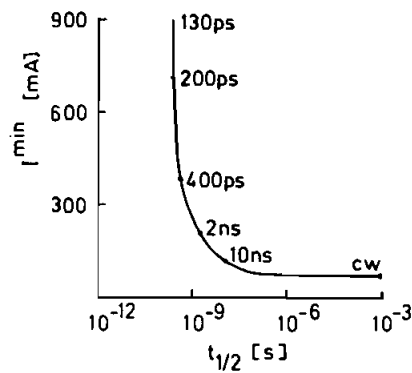


Figure 15. Measured minimum peak injection current for laser emission ('effective threshold') as a function of the current pulses at $T = 10^\circ\text{C}$ for GaAs DH laser.

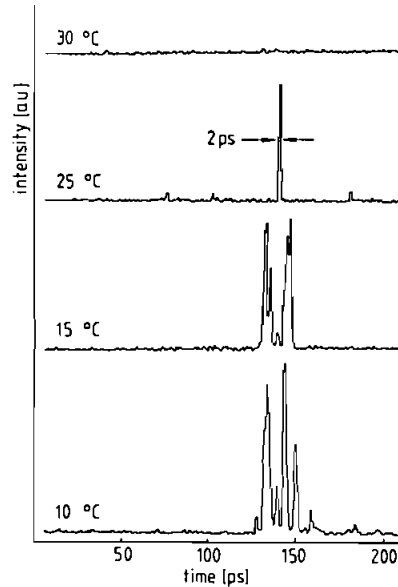


Figure 16. Light intensity versus time for different temperatures and for the dashed injection-current pulse of Fig. 9 at 6 dB attenuation, corresponding to peak current ratios $j_0 = 8.9$ (10°C), 8.6 (15°C), 8.1 (25°C), 7.8 (30°C).

At 10°C and at 15°C the emission consists of a number of closely spaced extremely narrow pulses, each of them having a halfwidth of a few picoseconds only. At 15°C the halfwidth of the envelope of these spikes is ≈ 15 ps. The total emission represents the first relaxation oscillation. A closer inspection shows that all spikes can be ordered to groups, where the time interval of members of the same group is roughly 9 ps and the same for all groups. Despite all other fluctuations, this time interval always remains the same. The interval is much smaller than the time difference to the second relaxation oscillation, which can hardly be seen any more under these injection conditions. The round-trip time of a pulse in the cavity is equal to 9 ps using an index of refraction $n = 3.7$. The spikes of one group are thus due to repetitive internal reflections of a single emission. The appearance of different groups might be caused by almost simultaneous 'ignition' at different points of the laser cavity. The intergroup time interval of a few picoseconds agrees with this interpretation. A further increase of the temperature to 25°C suppresses all spikes except one, having a width of 2 ps only. The amplitude and the delay time show some jitter.

The peak power of the laser is determined by a calibrated Si-photodiode. At 25°C the peak power is ≈ 1 mW and the energy of the pulse is $\approx 2 \times 10^{-15}$ J. At 15°C the energy is already one order of magnitude larger. The spectrum of the laser under these circumstances is already very broad and similar to CW spectra close to the threshold.

5.2. GaAs multiple-quantum-well laser

These lasers were developed at the research institute of the German post office using molecular-beam epitaxy. Figure 17 shows the structure of this laser type. The active layer consists of 5 GaAs quantum wells each 75 \AA thick, separated by 25 \AA

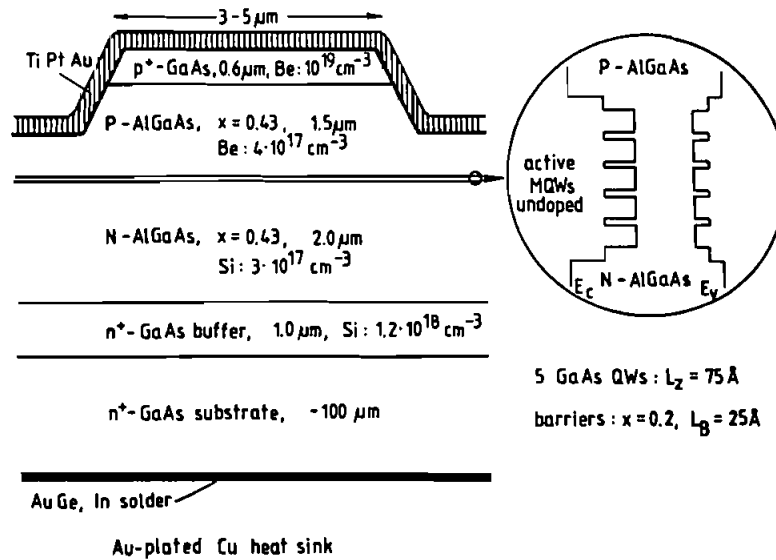


Figure 17. Structure of the GaAs multiple-quantum-well lasers used for our experiments.

thick $\text{Ga}_{0.8}\text{Al}_{0.2}\text{As}$ barriers. The CW threshold current density of these lasers is 600 A/cm^2 , corresponding to $I_t \approx 40 \text{ mA}$. Typically 4–5 longitudinal modes are emitted at a current of 50 mA. Quantum-well lasers in general have a larger gain and a lower threshold than conventional double-heterostructure lasers. This advantage results from the increased radiative recombination probability of the charge carriers, which are structurally localized in the wells (Christen *et al.* 1984).

Figure 18 shows 4 pulses emitted from such a laser held at 20°C after excitation with 200 ps/40 V pulses attenuated by 3–6 dB respectively. The time resolution of the streak camera is 8 ps. At 6 dB only the first relaxation oscillation with a width of 18 ps is emitted. The peak power is 200 mW and the pulse energy is 4 pJ. Subsequent pulses show almost no amplitude fluctuation, and the time jitter is below our resolution!

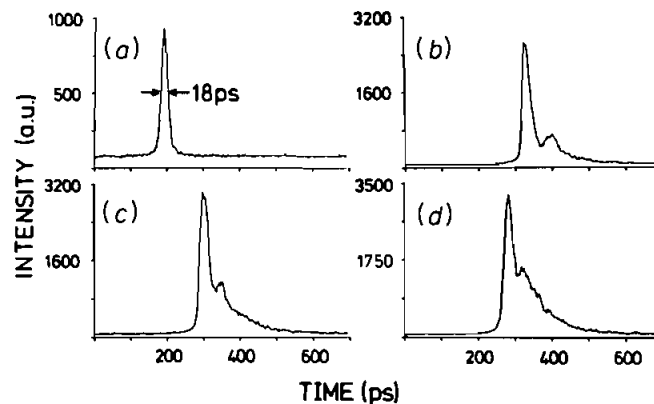


Figure 18. Light emission versus time from a MQW laser after excitation with 200 ps pulses. Resolution of the streak camera is 8 ps. Attenuation of the electrical pulses is (a) 6 dB, (b) 5 dB, (c) 4 dB, (d) 3 dB.

At 5 dB attenuation a second relaxation oscillation is emitted 40 ps after the first. The intensity of the first relaxation oscillation has increased by a factor of three (peak power 600 mW). By further increasing the current, the optical intensity again increases, albeit by a smaller amount. At 3 dB the second relaxation oscillation appears ≈ 34 ps after the first. The ratio of the amplitudes of subsequent relaxation oscillations is smaller than for the DH lasers investigated. The spectra show for all 4 cases clearly resolved longitudinal modes. The spectral width is only a factor of 5 larger than under CW emission condition.

A detailed study of the optimum condition for minimum temporal pulse width will be presented elsewhere (Ketterer *et al.* 1985).

5.3 InGaAsP/InP V-groove lasers

The lasers used here are structured in a similar way as the GaAs lasers discussed in § 5.1. They were also manufactured by AEG-Telefunken and are emitting at $1.23 \mu\text{m}$ or $1.26 \mu\text{m}$. Typical DC threshold currents are 150 mA. All experiments are carried out at a laser temperature of 20°C , which is controlled by a Peltier cooler. The photodetection system was described in § 4.2. Figure 19 shows the response of the detection system to $1.23 \mu\text{m}$ $\text{Ga}_x\text{In}_{1-x}\text{As}_y\text{P}_{1-y}$ laser pulses at three different values of the ratio of the injection peak current I to the DC threshold current I_t . A 250 ps/40 V pulse generator (see insert of Fig. 19) was used. With increasing I/I_t the second and following relaxation oscillations appear clearly as peaks or shoulders in the photocurrent.

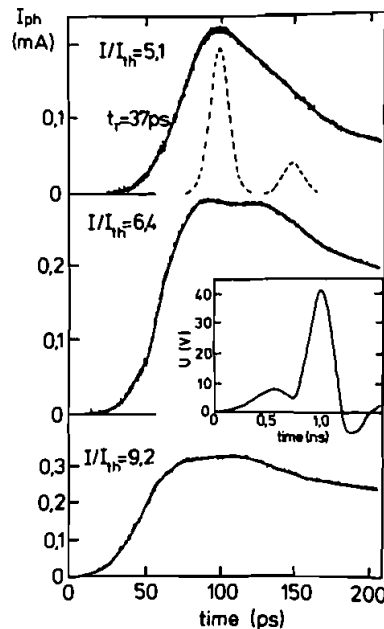


Figure 19. Photocurrent response I_{ph} of the detection system to $1.23 \mu\text{m}$ $\text{Ga}_x\text{In}_{1-x}\text{As}_y\text{P}_{1-y}$ laser pulses at three different J_0/J_t values. For $J_0/J_t = 5.1$ the deconvoluted laser pulses are shown. For the sake of clarity the deconvoluted pulse is shifted by ≈ 50 ps to later times.

The apparent spacing of the first two relaxation oscillations is ≈ 33 ps (at $I/I_1 = 6.4$). The risetime of the photocurrent pulse observed at $I/I_0 = 5.1$ is 37 ps.

The deconvolution procedure mentioned in §4.2 is employed in order to determine the true FWHM of the light pulses emitted by the laser, assuming a gaussian shape. The dashed lines in Fig. 19 show the result of this deconvolution for $I/I_1 = 5.1$. The FWHM of the first relaxation oscillation, which almost completely dominates the emission at this current, is found to be 15 ps. To the best of our knowledge this is by far the shortest light pulse generated to date at this wavelength by direct modulation of a semiconductor laser.

The observed FWHM is in agreement with theory (Schöll *et al.* 1984), which predicts a FWHM somewhat shorter than half of the spacing of the first two relaxation oscillations. The pulse energy and peak power of the first relaxation oscillation is determined from the response to a calibrated commercial germanium avalanche photodiode (Alcatel CG 4015), which has a sensitivity of 0.6 ± 0.2 A/W at $1.23 \mu\text{m}$ at a reverse bias of 10 V. For $I/I_1 = 5.1$ a pulse energy of 2.9 ± 0.9 pJ and a peak power of 200 ± 70 mW is found. More details will be published elsewhere (Bimberg *et al.* 1985).

6. Conclusion

The kinetics of generating ultrashort light pulses by gain modulation of unbiased semiconductor lasers emitting relaxation oscillations is modelled theoretically here and described using phase portraits. The halfwidth of the first relaxation oscillation is found to decrease below 10 ps in our model for typical GaAs DH laser parameters if sufficiently large and narrow current pulses are used for injection. The magnitude of the injection current, however, cannot be arbitrarily increased. Apart from technical problems, at large currents more than one relaxation oscillation is emitted and the overall width of the pulse train increases again. Minimum pulse width at maximum peak power is obtained for injection pulses of an optimum shape such that the second relaxation oscillation is just not yet triggered. It remains the problem of the experiment to generate such electrical pulses. To facilitate this task and to gain deeper physical insight in the most important laser-design parameters approximate analytical solutions for the width of the laser pulse, its intensity, and the delay time between optical and electrical pulse are derived.

Our experimental observations confirm the theoretical predictions extremely well. The key result of this paper is that, largely independently of the laser type, we are able to produce single laser pulses at high repetition rates up to 10 MHz typically 15 ps wide at a peak power of at least 200 mW. The pulses show very little amplitude and time jitter. We demonstrate this here for three different types of lasers: GaAs DH and MQW lasers emitting in the $0.8\text{--}0.9 \mu\text{m}$ range and InGaAsP DH lasers emitting in the $1.2\text{--}1.3 \mu\text{m}$ range. Since we are probably still not employing 'the optimum' injection pulse shape, there exists a further potential for decreasing the width. Indeed for some GaAs DH lasers we have observed pulses as narrow as 2 ps by tuning the laser operating temperature instead of the peak injection current. These pulses are much weaker (≈ 1 mW), however, and showed comparatively larger amplitude jitter.

Special injection pulse generating circuits and optical pulse detection systems for the two different wavelength ranges with temporal resolution in the picosecond range had to be developed to perform the experimental part of the work, and are

described in detail. The advantages of a full modulation of the laser current (no prebias) and an injection pulse shape independent of repetition frequency as used here are demonstrated.

The results of our time-resolved experiments and theoretical predictions are complementary to the recent exciting experimental results of Lau *et al.* (1984, 1985) and Onodera *et al.* (1984): using suitable lasers and pulse generators it should be possible to generate 10 ps or narrower pulses at repetition rates of 10 GHz which are still Fourier-transform-limited (show single longitudinal modes).

ACKNOWLEDGMENTS

We are very indebted to H. P. Vollmer from AEG-Telefunken, Ulm and to G. Weimann and W. Schlapp from FTZ Darmstadt for providing the excellent lasers. Thanks are due to P. Roentgen and H. Beneking, Institut für Halbleitertechnik, Aachen, who furnished the Ge detectors. M. Brezina was very helpful in assisting with an appreciable part of the experimental work.

REFERENCES

- AU YEUNG, J., 1981, Picosecond optical pulse generation at gigahertz rates by direct modulation of a semiconductor laser. *Appl. Phys. Lett.*, **38**, 308–310.
- BIMBERG, D., BÖTTCHER, E. H., KETTERER, K., VOLLMER, H. P., BENEKING, H., and ROENTGEN, P., 1985, Generation and detection of picosecond light pulses in the 1.2 μm –1.3 μm wavelength range. *Appl. Phys. Lett.* (accepted for publication).
- BIMBERG, D., KETTERER, K., SCHÖLL, E., and VOLLMER, H. P., 1984, Generation of 4 ps light pulses from directly modulated V-groove lasers. *Electron. Lett.*, **20**, 640–641.
- BOERS, P. M., VLAARDINGERBROEK, U. T., and DANIELSEN, M., 1975, Dynamic behaviour of semiconductor lasers. *Electron. Lett.*, **11**, 206–208.
- CHIK, K. D., DYMENT, J. C., and RICHARDSON, B. A., 1980, Self-sustained pulsations in semiconductor lasers: Experimental results and theoretical confirmation. *J. appl. Phys.*, **51**, 4029–4037.
- CHRISTEN, J., BIMBERG, D., STECKENBORN, A., and WEIMANN, G., 1984, Localisation induced electron-hole transition rate enhancement in GaAs quantum wells. *Appl. Phys. Lett.*, **44**, 84.
- DIXON, R. W., and JOYCE, W. B., 1979, Generalized expressions for the turn-on delay in semiconductor lasers. *J. appl. Phys.*, **50**, 4591–4595.
- HO, P. T., GLASSER, L. A., IPPEN, E. P., and HAUS, H. A., 1978, Picosecond pulse generation with a cw GaAlAs laser diode. *Appl. Phys. Lett.*, **33**, 241–242.
- HOLBROOK, U. B., SLEAT, W. E., and BRADLEY, D. J., 1980, Bandwidth limited picosecond pulse generation in an actively mode-locked GaAlAs diode laser. *Appl. Phys. Lett.*, **37**, 59–61.
- HWANG, C. J., and DYMENT, J. C., 1973, Dependence of threshold and electron lifetime on acceptor concentration in GaAs–Ga_{1-x}Al_xAs lasers. *J. appl. Phys.*, **44**, 3240–3244.
- IPPEN, E. P., and EILENBERGER, D. J., 1980, Picosecond pulse generation by passive mode locking of diode laser. *Appl. Phys. Lett.*, **37**, 267–269.
- ITO, H., YOKOYAMA, H., and INABA, H., 1980, Bandwidth limited picosecond optical pulse generation from actively mode-locked AlGaAs diode lasers. *Electron. Lett.*, **16**, 620–621.
- ITO, H., YOKOYAMA, H., MURATA, S., and INABA, H., 1979, Picosecond optical pulse generation from a RF-modulated AlGaAs DH diode laser. *Electron. Lett.*, **15**, 738–740.
- KETTERER, K., BIMBERG, D., BREZINA, M., SCHÖLL, E., WEIMANN, G., and SCHLAPP, W., 1985, Multiple quantum well lasers as efficient source for picosecond pulses. *Proc. 15th ESSDERC, Aachen 1985, Physica*, **129B**, 469.

- KLEIN, H. J., BIMBERG, D., and BENEKING, H., 1982a, Ultrafast thin film GaAs photoconductive detectors. *Thin Solid Films*, **92**, 273–279.
- KLEIN, H.-J., BIMBERG, D., BENEKING, H., KUHL, J., and GÖBEL, E. O., 1982b, High peak power picosecond light pulses from a direct modulated semiconductor laser. *Appl. Phys. Lett.*, **41**, 394–396.
- KRÄUTLE, H., ROENTGEN, P., and BENEKING, H., 1983, Epitaxial growth of Ge on GaAs substrates. *J. Cryst. Growth*, **65**, 439–443.
- LAU, K. Y., and YARIV, A., 1984, Self-sustained picosecond pulse generation in GaAlAs laser at an electrically tunable repetition rate by optoelectronic feedback. *Appl. Phys. Lett.*, **45**, 124–126.
- LAU, K. Y., YARIV, A., 1985, Ultra-high speed semiconductor lasers. *I.E.E.E. JI quant. Electron.*, **21**, 121–138.
- LIN, C., BURRUS, C. A., EISENSTEIN, G., TUCKER, R. S., BESOMI, P., and NELSON, R. J., 1984, 11.2 GHz picosecond optical pulse generation in gain-switched short-cavity InGaAsP injection lasers by high-frequency direct modulation. *Electron. Lett.*, **20**, 238–239.
- LUNDQVIST, S., ANDERSSON, T., ENG, S. T., 1983, Generation of tunable single-mode picosecond pulses from an AlGaAs-semiconductor laser with grating feedback. *Appl. Phys. Lett.*, **43**, 715–717.
- ONODERA, N., ITO, H., and INABA, H., 1984, FOURIER-transform-limited, single-mode picosecond optical pulse generation by a distributed feedback InGaAsP diode laser. *Appl. Phys. Lett.*, **45**, 843–845.
- SCHÖLL, E., BIMBERG, D., SCHUMACHER, H., and LANDSBERG, P. T., 1984, Kinetics of picosecond pulse generation in semiconductor lasers with bimolecular recombination at high current injection. *I.E.E.E. JI quant. Electron.*, **20**, 394–399.
- 'T HOOFT, G. W., 1981, The radiative recombination coefficient of GaAs from laser delay measurements and effective nonradiative carrier lifetimes. *Appl. Phys. Lett.*, **39**, 389–390.
- TSANG, W. T., OLSSON, N. A., and LOGAN, R. A., 1983, Mode-locked semiconductor lasers with gateable output and electrically controllable optical absorber. *Appl. Phys. Lett.*, **43**, 339–341.
- VAN DER ZIEL, J. P., 1981, Active mode-locking of double heterostructure lasers in an external cavity. *J. appl. Phys.*, **52**, 4435–4446.
- VAN DER ZIEL, J. P., and LOGAN, R. A., 1982, Generation of short optical pulses in semiconductor lasers by combined dc and microwave current injection. *I.E.E.E. JI quant. Electron.*, **18**, 1340–1350.
- VAN DER ZIEL, J. P., TSANG, W. T., LOGAN, R. A., MIKULYAK, R. M., and AUGUSTYNIAK, W. M., 1981, Subpicosecond pulses from passively mode-locked GaAs buried optical guide semiconductor lasers. *Appl. Phys. Lett.*, **39**, 525–527.
- WHITE, I. H., GALLAGHER, D. F. G., OSINSKI, M., and BOWLEY, D., 1985, Direct streak-camera observation of picosecond gain-switched optical pulses from a 1.5 μm semiconductor laser. *Electron. Lett.*, **21**, 197–199.